https://doi.org/10.5194/acp-2019-1026
Preprint. Discussion started: 20 December 2019

Atmospheric Chemistry and Physics
Discussions

Why the Indo-Gangetic Plain is the region with the largest NH_3 column in the globe during summertime?

Tiantian Wang[1], Yu Song[1], Zhenying Xu[1], Mingxu Liu[1], Tingting Xu[1,2], Wenling Liao[1], Lifei Yin[1], Xuhui Cai[1], Ling Kang[1], Hongsheng Zhang[3], Tong Zhu[1,4]

[1]State Key Joint Laboratory of Environmental Simulation and Pollution Control, Department of Environmental Science, Peking University, Beijing 100871, China
[2]Environmental College, Chengdu University of Technology, Chengdu 610059, China
[3]Laboratory for Climate and Ocean-Atmosphere Studies, Department of Atmospheric and Oceanic Sciences, School of Physics, Peking University, Beijing 100871, China
[4]Beijing Innovation Center for Engineering Science and Advance Technology, Peking University, Beijing 100871, China

Correspondence to: Yu Song (songyu@pku.edu.cn)

Abstract. Satellite observations show a global maximum in ammonia (NH_3) over the Indo-Gangetic Plain (IGP), with a peak in summer. However, it has never been explained explicitly. In this study, we investigated the causes of high NH_3 loading over the IGP in summer using WRF-Chem (Weather Research and Forecasting model coupled to chemistry). IGP has relatively high NH_3 emission fluxes (0.4 t km^{-2} $month^{-1}$) due to intensive agricultural activities and high air temperature in summer. Additionally, low sulfur dioxide (SO_2) and nitrogen oxides (NO_x) emissions and high air temperature limit the gas-to-particle conversion of NH_3, particularly for ammonium nitrate formation. Moreover, the barrier effects of the Himalayas in combination with the surface convergence weaken the horizontal diffusion of NH_3. The high NH_3 loading over the IGP mainly results from the low gas-to-particle partitioning of NH_3 caused by low SO_2 and NO_x emissions. It contrasts to those in the North China Plain, where high SO_2 and NO_x emissions promote the conversion of gaseous NH_3 into particulate ammonium.

1 Introduction

Ammonia (NH_3) has multiple environmental implications. As the only alkaline gas in the atmosphere, it reacts with sulfuric acid (H_2SO_4) or nitric acid (HNO_3) to produce ammonium (NH_4^+) containing aerosols (Seinfeld and Pandis, 2006), which can affect Earth's radiative balance (Abbatt et al., 2006;Adams et al., 2001) and endanger public health (Pope et al., 2002;Stokstad, 2014). In addition, NH_3 is the main form of reactive nitrogen in the environment (Reis et al., 2009), the deposition of ammonia and ammonium can cause acidification of terrestrial ecosystems and eutrophication of water bodies (Paerl et al., 2014).

Satellite observations (Van Damme et al., 2018;Warner et al., 2016) and ground-based measurements (Carmichael et al., 2003) have revealed that the Indo-Gangetic Plain (IGP) has the global maximum NH_3 loading, particularly during summer. Previous studies have suggested that the high NH_3 loading over the IGP during summer is caused by high NH_3 emissions from intensive agricultural activities(Clarisse et al., 2009;Van Damme et al., 2015b). Interestingly, satellite measurements show that the total columns of NH_3 over the IGP are much higher than those over the North China Plain (NCP), which has higher NH_3 emissions fluxes (www.meicmodel.org/dataset-mix). Therefore, emissions alone might not be enough to explain the high NH_3 loading over the IGP.

Apart from dry deposition and wet removal by precipitation, another main sink for NH_3 is scavenging by acidic species to form particulate NH_4^+. H_2SO_4 and HNO_3 resulting from the oxidation of sulfur dioxide (SO_2) and nitrogen oxides (NO_x) are major acidic species in the atmosphere. Previous studies have confirmed that reduced SO_2 and NO_x emissions are key factors driving the increase in NH_3 concentration (Liu et al., 2018;Yu et al., 2018;Warner et al., 2017). In addition, meteorological conditions (including wind speed, precipitation, relative humidity and air temperature) also influence NH_3 loading through various chemical and physical processes. These factors may be causing the high NH_3 loading over the IGP, but these assumptions have not been verified in a modeling study.

In this study, we use a regional air quality model to investigate the causes of high NH_3 loading over the IGP during summer. This is the first study to analyze the causes of high NH_3 loading over the IGP considering all possible factors. The remainder of this paper is organized as follows. The air quality model and observational data are described in sect. 2. Section 3 analyzes the influences of several factors (including emissions, chemical conversion, and meteorological conditions) on NH_3 loading. Among them, SO_2 and NO_x emissions over the IGP are compared to those over the NCP to clearly illustrate their impacts on NH_3 loading. Section 4 provides concluding remarks.

2 Methods

2.1 WRF-Chem model and emissions inventory

WRF-Chem (Fast et al., 2006;Grell et al., 2005) version 3.6.1 was applied to investigate the cause of the high NH_3 loading over the IGP during summer. The simulation was performed on a domain with 30 km horizontal resolution covering the northern part of India and parts of Pakistan, Nepal, China, and Bangladesh with 120 × 90 grid cells. There were 23 vertical levels from the surface to the top pressure of 50 hPa. June to August was considered summer. The simulations were conducted from 25 May to 31 August 2010 and the first 7 days (25-31 May) were treated as the spin-up period. The initial meteorological and boundary conditions were obtained from the National Centers for Environmental Prediction Final Analysis with a 6 h temporal resolution. The detailed model configurations are described in Table S1.

Anthropogenic emissions were obtained from the MIX inventory (Li et al., 2017), an Asian anthropogenic emissions inventory that harmonizes several local inventories using a mosaic approach. MIX uses Regional Emissions Inventory in Asia (REAS2, version 2) (Kurokawa et al., 2013) for NH_3 emissions in India.

2.2 Observational dataset

Atmospheric total columns of NH_3 were derived from measurements of an Infrared Atmospheric Sounding Interferometer (IASI) on board MetOp-A (https://iasi.aeris-data.fr/NH3/). Metop-A was launched in 2006 in a Sun-synchronous orbit with a mean local solar overpass time of 9:30 a.m. and 9:30 p.m. Only the daytime measurements have been used here, because the nighttime measurements had larger relative errors caused by the general lower thermal contrast for the nighttime overpass (Van Damme et al., 2014). It has been found that the IASI samples at the overpass time could represent the entire day, and

https://doi.org/10.5194/acp-2019-1026
Preprint. Discussion started: 20 December 2019

IASI NH_3 observations are in fair agreement with ground-based measurements (Dammers et al., 2016;Van Damme et al., 2015a).This work used the ANNI-NH3-v2.2R-I retrieval product, which relied on ERA-Interim reanalysis for its meteorological inputs (Van Damme et al., 2017). The seasonal mean NH_3 column concentrations over East Asia on a 0.25° × 0.25° grid in summer 2010 have been determined based on the relative error weighting mean method (Van Damme et al., 2014).

Meteorological data at 38 sites over northern India obtained from the National Climate Data Center (https://gis.ncdc.noaa.gov/maps/ncei/cdo/hourly) were used to evaluate the accuracy of meteorological simulations. The evaluated variables included hourly wind speed at 10 m (WS10), wind direction at 10 m (WD10), relative humidity at 2 m (RH2) and temperature at 2 m (T2). The statistical parameters included the mean bias (MB), normalized mean bias (NMB), root mean square error (RMSE) and correlation coefficient (R). In addition, air temperature at 21 sites over the NCP obtained from the National Climate Data Center were also used in this work.

2.3 ISORROPIA-II thermodynamic model

The thermodynamic equilibrium model, ISORROPIA-II (Fountoukis and Nenes, 2007), treating the thermodynamics of NH_4^+-SO_4^{2-}-NO_3^--K^+-Ca^{2+}-Mg^{2+}-Na^+-Cl^--H_2O aerosol system, was used to investigate the influence of air temperature on the NH_3 total columns. In this study, ISORROPIA-II was run in the “forward mode” and assuming particles are “metastable” with no solid precipitates. As inputs of ISORROPIA-II, the outputs (water-soluble ions, gas species, T and RH) of WRF-Chem were first averaged over the IGP and then averaged for summer 2010. Using ISORROPIA-II, we simulated 20 scenarios. In these cases, air temperature of each layer increased or decreased by 10 °C synchronously, with the interval of 1 °C. Meanwhile, the other input parameters remained the same. Then, we calculated the columnar $\varepsilon(NH_4^+)$ (partitioning ratios of NH_4^+ to total ammonia (TA, TA = NH_3 + NH_4^+)) in each case. The columnar $\varepsilon(NH_4^+)$ is the sum of the $\varepsilon(NH_4^+)$ of each vertical level, but each weighted by the thickness of the layer and mass concentration of TA.

3 Results

3.1 High NH_3 emissions

IGP is a vast stretch of fertile alluvial plain spanning the banks of the Indus and Ganges Rivers and their tributaries. The main part of the IGP is located in India. The estimated NH_3 emissions in India in 2010 was 9.9 Tg, which is comparable to that in China (9.8 Tg) and accounts for about 34 % of total NH_3 emissions in Asia (Li et al., 2017). Agriculture is the largest NH_3 emitter in India, accounting for about 76 % of the total NH_3 emissions (Li et al., 2017). Agricultural NH_3 emissions mainly originate from animal husbandry and fertilizer application (Bouwman et al., 1997;Streets et al., 2003). India is the second largest N-fertilizer consumer (after China) and consumes 16.5 Tg N-fertilizers (16 % of the world’s total) (FAOSTAT, 2010). In addition, there are an estimated 302 million cattle and buffalo in India (19 % of world’s total), which is more than any other country (FAOSTAT, 2010). It is estimated that cattle and buffalo account for about 80 % of NH_3 emissions among livestock in India (Aneja et al., 2012).

NH_3 emissions over the IGP was 4.3 Tg in 2010 (estimated using the MIX database), which was mainly attributed to intensive agricultural practices. The IGP is known as the food bowl of India spreading across the states of Punjab, Haryana, Uttar Pradesh, Bihar, and West Bengal (blue quadrangle in Fig. 1). The total number of cattle and buffalo in the five states was estimated to be 103 million (34 % of the national total) in 2012 (19th Livestock Census 2012, 2012). The total amount of N-fertilizer applied in the five states was estimated to be 6.9 Tg (42 % of the national total) in 2010 (Agricultural Statistics At a Glance 2012, 2012a). NH_3 emissions over the IGP in summer are very high with a regional mean NH_3 emissions flux of 0.4 t km^{-2} $month^{-1}$ (estimated using MIX database for 2010). This is consistent with satellite observations, which also show a summer peak of NH_3 columns over the IGP (Van Damme et al., 2015b). The summer peak of NH_3 emissions over the IGP might be the joint result of intensive N-fertilizer applications and high temperature. Summer is the sowing season in the IGP, when a large amount of N-fertilizer applied to the cropland as base fertilizer (Agricultural Statistics At a Glance 2012, 2012a). In addition, the summer air temperature is very high over the IGP with an observed regional mean value of 30.9 °C in summer 2010. Ammonia emissions increase exponentially with temperature (Riddick et al., 2016). The high application rate of N-fertilizer and high air temperature could cause high NH_3 emissions, resulting in the high NH_3 columns.

The spatial distribution of seasonal mean NH_3 total columns over East Asia during summer 2010 is shown in Fig. 1. The NH_3 columns over the IGP (7.6×10^{16} molecules cm^{-2}) were about twice as large as what was observed over the NCP (4.1×10^{16} molecules cm^{-2}) in summer 2010. The NCP is also a large agricultural region (Huang et al., 2012). The regional mean NH_3 emissions flux over the NCP was 0.7 t km^{-2} $month^{-1}$ in summer 2010 (estimated using the MIX database), which was about 1.8 times that of the IGP. The IGP has much higher NH_3 total columns (Fig. 1) compared to the NCP, but lower NH_3 emissions fluxes (Fig. S1a). Therefore, other factors might lead to the high NH_3 loading over the IGP in summer besides high NH_3 emissions.

3.2 Low gas-to-particle conversion of NH_3

The emissions fluxes of SO_2 and NO_x (both are 0.3 t km^{-2} $month^{-1}$) over the IGP are only about one-fourth of that over the NCP (1.1 and 1.3 t km^{-2} $month^{-1}$) (Table 1 and Fig. S1). The relatively low SO_2 and NO_x emissions could be an important factor causing the high NH_3 columns over the IGP. In this study, we used the molar ratio (R_{emis}) of NH_3 emissions fluxes (E_A) to the sum of twice the SO_2 emissions fluxes (E_S) and NO_x emissions fluxes (E_N) to roughly represent the richness of NH_3 in the atmosphere, given by Eq. (1):

$$R_{emis} = \frac{E_A}{2 \times E_S + E_N} . \quad (1)$$

The calculated R_{emis} in the IGP was 1.35, which was about 2.6 times as large as that in the NCP (0.51). We performed simulations for a base case and a 'increased SO_2/NO_x emissions' case to investigate the impact of SO_2 and NO_x emissions on

NH_3 loading. In the increased SO_2/NO_x emissions case, the emissions of SO_2 and NO_x increased 2.6 times to make R_{emis} of the IGP equal to that of the NCP.

The simulated NH_3 columns in the base case are shown in Fig. 2a. The regional mean NH_3 total column over the IGP from the base case was 8.8×10^{16} molecules cm^{-2}. It is noted that the IASI NH_3 columns cannot be quantitatively compared to modeled NH_3 columns as the IASI NH_3 products do not provide information on the vertical sensitivity to properly weight the model values. Nonetheless, the spatial distribution of the NH_3 columns in the base run was consistent with the satellite observations, both of which showed the highest values in northwestern IGP (Figs. 1 and 2a). The statistical performance of the meteorological predictions at 38 sites over Northern India are presented in Table S2. The predicted T2 matched well with the observations with a correlation coefficient of 0.8 and an NMB of 4.2 %. The predicted RH2 was slightly underestimated with an NMB of –13.4 % and a correlation coefficient of 0.8. The predicted WS10 agreed reasonably well with the observations with an NMB of –5.3 %. In addition, the simulated WD10 matched well with the observations, and both the predicted and observed dominant wind direction was SSE. The good agreement between the simulation and the observations confirms the reliability of the meteorological prediction over the simulation domain.

The spatial distribution of the NH_3 total column in the increased emissions case is shown in Fig. 2b. The NH_3 total columns significantly decreased over the entire IGP, with a regional mean value of 2.5×10^{16} molecules cm^{-2} (a 72.2 % decrease compared to the base case). The surface $\varepsilon(NH_4^+)$ in the base case and the increased SO_2/NO_x emissions case are shown in Fig. 2 (panels c and d, respectively). The surface $\varepsilon(NH_4^+)$ in the base case was fairly low with a regional mean value of 0.3 over the IGP, close to the observations in Delhi (0.4 in summer 2010) (Singh and Kulshrestha, 2012). In the increased SO_2/NO_x emissions case, the regional mean surface $\varepsilon(NH_4^+)$ increased to 0.6 over the IGP. Significant increases in surface SO_4^{2-} and NO_3^- concentrations were also found (Fig. S2). The regional mean surface SO_4^{2-} and NO_3^- concentrations increased from 9.7 to 24.9 and from 7.2 to 20.0 µg m^{-3}, respectively. Additionally, the regional mean columnar $\varepsilon(NH_4^+)$ over the IGP is 0.56 in the base case and increases to 0.87 in the increased SO_2/NO_x emissions case. This suggests that the increased SO_2 and NO_x emissions enhanced the formation of acidic species and promoted the conversion of NH_3 into NH_4^+. The effectively reduced NH_3 total columns in the increased SO_2/NO_x emissions case indicate that low SO_2 and NO_x emissions could be the major cause of the high NH_3 loading over the IGP.

Besides the amount of acidic species, air temperature is also an important factor affecting the thermodynamic equilibrium of NH_3 between the gas phase and the particle phase. Higher air temperature limits the gas-to-particle conversion of NH_3 and enhances volatilization of NH_4NO_3 (Seinfeld and Pandis, 2006). The observed regional mean air temperature over the IGP in summer 2010 was 30.9 °C, about 4.9 °C higher than the NCP (26.0 °C). Thermodynamic calculation was conducted using ISORROPIA-II based on WRF-Chem outputs (The detailed descriptions are in Sect. 2.3). As shown in Fig. 3, the columnar $\varepsilon(NH_4^+)$ increases as temperature decreases. A 10°C decrease in temperature results in a 0.07 increase in $\varepsilon(NH_4^+)$ and a consequent 17 % decrease in NH_3 total columns. Additionally, a 10°C increase in temperature results in a 0.08 decrease in $\varepsilon(NH_4^+)$ and a consequent 20 % increase in NH_3 total columns. If the temperature over the IGP drops to the temperature typical of the NCP (a 4.9 °C decrease), the NH_3 total columns over the IGP will only decrease by 10 %. In contrast, if the SO_2/NO_x

https://doi.org/10.5194/acp-2019-1026
Preprint. Discussion started: 20 December 2019

emissions over the IGP increase to make the R_{emis} of the IGP equal to that of the NCP, the NH_3 column over the IGP will decrease by 72.2 %. Therefore, the low SO_2/NO_x emissions have a greater effect on causing high NH_3 columns over the IGP than the high air temperature.

3.2 Weak horizontal diffusion of NH_3

The IGP is located in the northern part of the Indian subcontinent and is surrounded by unique topography with the Himalayan range to the north and the Sulaiman range to the west. Weather on the Indian subcontinent is controlled by the low-level Indian monsoon regime from June through September (Lawrence and Lelieveld, 2010). Fig. 4a shows the spatial distributions of surface wind flow and wind speed in summer 2010. The dominant wind direction is southwest over the Indian peninsula and southeast over the IGP. Air mainly flows from the west coast of India and the south coast of Bengal. Surface wind speed is high on the west coast of India (>5 m s^{-1}) and on the south coast of Bengal (>4 m s^{-1}) but decreases from the coast inland. Mountains serve as barriers to the airflow on the surface of the Earth (Barry, 2008). Chow et al. (2013) reported that when stably stratified airflow encounters an extra-tropical mountain barrier, it is forced to rise and cool adiabatically. Consequently, higher pressure along the slope could be created, which could decelerate and block the flow. After a while, geostrophic adjustment occurs. As a result, the airflow turns left (right) in the northern (southern) hemisphere, and a barrier jet blowing parallel to the barrier is formed. As shown in Fig. 4a, the southerly airflow from the Bay of Bengal turns left when approaching the Himalayas, and then an easterly barrier jet parallel to the Himalayas is formed. The southwesterly airflow from the west coast of India also turns left when approaching the Himalayas. Similarly, wind flow at 850 hPa (Fig. 4b) also shows left-turning airflow near the Himalayas. The left-turning airflow indicates that the barrier effect of the Himalayas limits the northward movement of polluted air. Both satellite observations and the model simulation show that the high NH_3 columns over the IGP are effectively cut off by mountains to the north (Fig. 2a and Fig. S3).

As shown in Fig. 4b, an area of low geopotential height extends from Pakistan to east India following the IGP. This elongated region of low pressure is known as the monsoon trough (Bohlinger et al., 2017). It causes wind to converge over this region. The convergence of horizontal wind can be observed from wind flow at both the surface and at 850 hPa. The prevailing wind directions south and east of the IGP are southwest and southeast, respectively. As a result of convergence of horizontal winds, an area of low wind speed forms and covers most of the IGP. The regional mean surface wind speed over the IGP is <3 m s^{-1}. The weak wind speed in association with the convergence weakens the horizontal advection of NH_3 and results in the accumulation of NH_3 over the IGP.

The ventilation rate (V_r) of the four edges of the IGP was used to illustrate the accumulation of an air mass over the IGP (Fig. 4d). The V_r of one edge is defined as the product of sectional area to the transport wind, given by Eq. (2):

$$V_r = AU_T \quad (2)$$

The sectional area A can be expressed as A = ZL, where Z is the mean boundary layer height along the edge and L is the length of the edge. The transport wind U_T is given by $U_T = \frac{1}{m}\sum_{j=1}^{m}\left(\frac{1}{n}\sum_{i=1}^{n}U_{ij}\right)$. m and n are the number of locations along the edge and vertical levels within the ABL where the winds are measured or predicted. U_{ij} is the wind speed perpendicular to the cross-section at each height and location along the edge. The ventilation rates of the four edges of the IGP were calculated using the WRF-Chem simulation results. The total V_r of the inflow from the southern and eastern edges (3.1×10^9 m^3 s^{-1}) was 64 % higher than the total V_r of the outflow from the western and northern edges (1.9×10^9 m^3 s^{-1}). The strong inflow and weak outflow indicate accumulation of the air mass over the IGP in summer. Therefore, outward transport of NH_3 from the IGP through horizontal advection could be weak.

Interestingly, both relative humidity and precipitation are high over the IGP (Figs. S4), with regional mean values of 63 % and 660 mm during summer 2010. The high relative humidity and precipitation suggest strong gas-to-particle conversion and wet scavenging of NH_3 (Seinfeld & Pandis, 2006). The observed high NH_3 loading under such a wet condition further indicates the effectiveness of other factors leading to high NH_3 loading. The meteorological conditions in the northwest IGP are characterized by higher air temperature, lower humidity, and lower rainfall compared to the southeast IGP (Figs. 4c and S4), all of which are conducive to the increase of NH_3. Consistently, NH_3 total columns decrease from northwest to southeast along the IGP as revealed by both the satellite measurements and model simulations (Figs. 1 and 2a). However, emission fluxes of NH_3 over the northwest IGP are also obviously higher than the southeast IGP (Fig. S1). To exclude the impact of emissions on the spatial distributions of NH_3, simulations for a "homogeneous emissions" case was performed by using WRF-Chem, where emissions of all primary pollutants over the IGP were set to their regional mean values. As shown in Fig. 5, NH_3 total columns in the homogeneous emissions case still appear to decrease from northwest to southeast along the IGP. It is indicated that the meteorological factors (atmospheric diffusion, temperature, relative humidity, and precipitation) are important causes of the higher NH_3 loadings over the northwest IGP than the southeast IGP.

4 Conclusions

Satellite observations have revealed that the IGP has the global maximum NH_3 loading with a peak in summer. Our study reveals that the high NH_3 loading over the IGP appears to be the joint result of high NH_3 emissions, weak chemical loss, and weak horizontal diffusion. Intensive agricultural activities in combination with high temperature resulted in relatively high NH_3 emissions over the IGP, with a regional mean NH_3 emissions flux of 0.4 t km^{-2} month^{-1}. The low SO_2 and NO_x emissions and high temperature limited the conversion of NH_3 to NH_4^+. The low chemical loss of gaseous NH_3 is a key reason for the high NH_3 loading over the IGP. In addition, orographic and meteorological conditions also play important roles in NH_3 accumulation over the IGP. The barrier effects of the Himalayas limit the northward movement of monsoon air in summer.

The low wind speed (<3 m s^{-1}) in association with the surface convergence over the IGP weakens horizontal diffusion, which is conducive to the accumulation of NH_3 over the IGP.

Data availability

The IASI data used in this study was provided by the AERIS data infrastructure (https://iasi.aeris-data.fr/NH3/). The meteorological data used in this study was obtained from the National Climate Data Center integrated surface database (https://gis.ncdc.noaa.gov/maps/ncei/cdo/hourly). The anthropogenic emissions are available from MIX inventory (www.meicmodel.org/dataset-mix).

Author contribution

Y.S initiated the investigation. T.W performed the modelling analyses. T.W, Y.S, Z.X and T.Z wrote and edited the manuscript. M.L, T.X, W.L, L.Y, X.C, H.Z and L.K contributed to discussions of the results and the manuscript.

Competing interests

The authors declare no competing interests.

Acknowledgements

This work was supported by the National Natural Science Foundation of China (NSFC) (91644212, 41675142 and 91837209) and the National Key R&D Program of China (2016YFC0201505).

References

Agricultural Statistics At a Glance 2012, Department of Agriculture and Cooperation, Ministry of Agriculture, Government of India, https://eands.dacnet.nic.in/latest_2012.htm, 2012.

19th Livestock Census 2012, Department of Animal Husbandry, Dairying & Fisheries, Ministry of Agriculture, Government of India, http://dahd.nic.in/about-us/divisions/statistics, 2012.

Abbatt, J. P. D., Benz, S., Cziczo, D. J., Kanji, Z., Lohmann, U., and Mohler, O.: Solid ammonium sulfate aerosols as ice nuclei: A pathway for cirrus cloud formation, Science, 313, 1770-1773, 10.1126/science.1129726, 2006.

Adams, P. J., Seinfeld, J. H., Koch, D., Mickley, L., and Jacob, D.: General circulation model assessment of direct radiative forcing by the sulfate-nitrate-ammonium-water inorganic aerosol system, J. Geophys. Res. Atmos., 106, 1097-1111, 10.1029/2000jd900512, 2001.

Aneja, V. P., Schlesinger, W. H., Erisman, J. W., Behera, S. N., Sharma, M., and Battye, W.: Reactive nitrogen emissions from crop and livestock farming in India, Atmos. Environ., 47, 92-103, 10.1016/j.atmosenv.2011.11.026, 2012.

Barry, R. G.: Mountain Weather and Climate, Third Edition, Cambridge University Press, Cambridge, 2008.

Bohlinger, P., Sorteberg, A., and Sodemann, H.: Synoptic Conditions and Moisture Sources Actuating Extreme Precipitation in Nepal, J. Geophys. Res. Atmos., 122, 12653-12671, 10.1002/2017jd027543, 2017.

Bouwman, A. F., Lee, D. S., Asman, W. A. H., Dentener, F. J., VanderHoek, K. W., and Olivier, J. G. J.: A global high-resolution emission inventory for ammonia, Global. Biogeochem. Cy., 11, 561-587, 10.1029/97gb02266, 1997.

Carmichael, G. R., Ferm, M., Thongboonchoo, N., Woo, J. H., Chan, L. Y., Murano, K., Viet, P. H., Mossberg, C., Bala, R., Boonjawat, J., Upatum, P., Mohan, M., Adhikary, S. P., Shrestha, A. B., Pienaar, J. J., Brunke, E. B., Chen, T., Jie, T., Guoan, D., Peng, L. C., Dhiharto, S., Harjanto, H., Jose, A. M., Kimani, W., Kirouane, A., Lacaux, J. P., Richard, S., Barturen, O., Cerda, J. C., Athayde, A., Tavares, T., Cotrina, J. S., and Bilici, E.: Measurements of sulfur dioxide, ozone and ammonia concentrations in Asia, Africa, and South America using passive samplers, Atmos. Environ., 37, 1293-1308, 10.1016/S1352-2310(02)01009-9, 2003.

Chow, F. K., Wekker, S. F. J. D., and Snyder, B. J.: Mountain Weather Research and Forecasting Recent Progress and Current Challenges, Springer, Dordrecht, 2013.

Clarisse, L., Clerbaux, C., Dentener, F., Hurtmans, D., and Coheur, P. F.: Global ammonia distribution derived from infrared satellite observations, Nat. Geosci., 2, 479-483, 10.1038/ngeo551, 2009.

Dammers, E., Palm, M., Van Damme, M., Vigouroux, C., Smale, D., Conway, S., Toon, G. C., Jones, N., Nussbaumer, E., Warneke, T., Petri, C., Clarisse, L., Clerbaux, C., Hermans, C., Lutsch, E., Strong, K., Hannigan, J. W., Nakajima, H., Morino, I., Herrera, B., Stremme, W., Grutter, M., Schaap, M., Kruit, R. J. W., Notholt, J., Coheur, P. F., and Erisman, J. W.: An evaluation of IASI-NH_3 with ground-based Fourier transform infrared spectroscopy measurements, Atmos. Chem. Phys., 16, 10351-10368, 10.5194/acp-16-10351-2016, 2016.

FAOSTAT. Statistical Database of Food and Agriculture Organization of the United Nations, The Food and Agriculture Organization of the United Nations, http://faostat.fao.org/, 2010.

Fast, J. D., Gustafson, W. I., Easter, R. C., Zaveri, R. A., Barnard, J. C., Chapman, E. G., Grell, G. A., and Peckham, S. E.: Evolution of ozone, particulates, and aerosol direct radiative forcing in the vicinity of Houston using a fully coupled meteorology-chemistry-aerosol model, J. Geophys. Res. Atmos., 111, 10.1029/2005jd006721, 2006.

Fountoukis, C., and Nenes, A.: ISORROPIA II: a computationally efficient thermodynamic equilibrium model for K^+-Ca^{2+}-Mg^{2+}-NH_4^+-Na^+-SO_4^{2-}-NO_3^--Cl^--H_2O aerosols, Atmos. Chem. Phys., 7, 4639-4659, 10.5194/acp-7-4639-2007, 2007.

Grell, G. A., Peckham, S. E., Schmitz, R., McKeen, S. A., Frost, G., Skamarock, W. C., and Eder, B.: Fully coupled "online" chemistry within the WRF model, Atmos. Environ., 39, 6957-6975, 10.1016/j.atmosenv.2005.04.027, 2005.

Huang, X., Song, Y., Li, M. M., Li, J. F., Huo, Q., Cai, X. H., Zhu, T., Hu, M., and Zhang, H. S.: A high-resolution ammonia emission inventory in China, Global. Biogeochem. Cy., 26, 10.1029/2011gb004161, 2012.

Kurokawa, J., Ohara, T., Morikawa, T., Hanayama, S., Janssens-Maenhout, G., Fukui, T., Kawashima, K., and Akimoto, H.: Emissions of air pollutants and greenhouse gases over Asian regions during 2000-2008: Regional Emission inventory in ASia (REAS) version 2, Atmos. Chem. Phys., 13, 11019-11058, 10.5194/acp-13-11019-2013, 2013.

Lawrence, M. G., and Lelieveld, J.: Atmospheric pollutant outflow from southern Asia: a review, Atmos. Chem. Phys., 10, 11017-11096, 10.5194/acp-10-11017-2010, 2010.

Li, M., Zhang, Q., Kurokawa, J., Woo, J. H., He, K. B., Lu, Z. F., Ohara, T., Song, Y., Streets, D. G., Carmichael, G. R., Cheng, Y. F., Hong, C. P., Huo, H., Jiang, X. J., Kang, S. C., Liu, F., Su, H., and Zheng, B.: MIX: a mosaic Asian anthropogenic emission inventory under the international collaboration framework of the MICS-Asia and HTAP, Atmos. Chem. Phys., 17, 935-963, 10.5194/acp-17-935-2017, 2017.

Liu, M. X., Huang, X., Song, Y., Xu, T. T., Wang, S. X., Wu, Z. J., Hu, M., Zhang, L., Zhang, Q., Pan, Y. P., Liu, X. J., and Zhu, T.: Rapid SO_2 emission reductions significantly increase tropospheric ammonia concentrations over the North China Plain, Atmos. Chem. Phys., 18, 17933-17943, 10.5194/acp-18-17933-2018, 2018.

Paerl, H. W., Gardner, W. S., McCarthy, M. J., Peierls, B. L., and Wilhelm, S. W.: Algal blooms: Noteworthy nitrogen, Science, 346, 175-175, 10.1126/science.346.6206.175-a, 2014.

Pope, C. A., Burnett, R. T., Thun, M. J., Calle, E. E., Krewski, D., Ito, K., and Thurston, G. D.: Lung cancer, cardiopulmonary mortality, and long-term exposure to fine particulate air pollution, Jama-J. Am. Med. Assoc., 287, 1132-1141, 10.1001/jama.287.9.1132, 2002.

Reis, S., Pinder, R. W., Zhang, M., Lijie, G., and Sutton, M. A.: Reactive nitrogen in atmospheric emission inventories, Atmos. Chem. Phys., 9, 7657-7677, 10.5194/acp-9-7657-2009, 2009.

Riddick, S., Ward, D., Hess, P., Mahowald, N., Massad, R., and Holland, E.: Estimate of changes in agricultural terrestrial nitrogen pathways and ammonia emissions from 1850 to present in the Community Earth System Model, Biogeosciences, 13, 3397-3426, 10.5194/bg-13-3397-2016, 2016.

Seinfeld, J. H., and Pandis, S. N.: Atmospheric Chemistry and Physics: From Air Pollution to Climate Change, John Wiley, New York, 2006.

Singh, S., and Kulshrestha, U. C.: Abundance and distribution of gaseous ammonia and particulate ammonium at Delhi, India, Biogeosciences, 9, 5023-5029, 10.5194/bg-9-5023-2012, 2012.

Stokstad, E.: AIR POLLUTION Ammonia Pollution From Farming May Exact Hefty Health Costs, Science, 343, 238-238, 10.1126/science.343.6168.238, 2014.

Streets, D. G., Bond, T. C., Carmichael, G. R., Fernandes, S. D., Fu, Q., He, D., Klimont, Z., Nelson, S. M., Tsai, N. Y., Wang, M. Q., Woo, J. H., and Yarber, K. F.: An inventory of gaseous and primary aerosol emissions in Asia in the year 2000, J. Geophys. Res. Atmos., 108, 10.1029/2002jd003093, 2003.

Van Damme, M., Clarisse, L., Heald, C. L., Hurtmans, D., Ngadi, Y., Clerbaux, C., Dolman, A. J., Erisman, J. W., and Coheur, P. F.: Global distributions, time series and error characterization of atmospheric ammonia (NH_3) from IASI satellite observations, Atmos. Chem. Phys., 14, 2905-2922, 10.5194/acp-14-2905-2014, 2014.

Van Damme, M., Clarisse, L., Dammers, E., Liu, X., Nowak, J. B., Clerbaux, C., Flechard, C. R., Galy-Lacaux, C., Xu, W., Neuman, J. A., Tang, Y. S., Sutton, M. A., Erisman, J. W., and Coheur, P. F.: Towards validation of ammonia (NH_3) measurements from the IASI satellite, Atmos Meas Tech, 8, 1575-1591, 10.5194/amt-8-1575-2015, 2015a.

Van Damme, M., Erisman, J. W., Clarisse, L., Dammers, E., Whitburn, S., Clerbaux, C., Dolman, A. J., and Coheur, P. F.: Worldwide spatiotemporal atmospheric ammonia (NH_3) columns variability revealed by satellite, Geophys. Res. Lett., 42, 8660-8668, 10.1002/2015gl065496, 2015b.

Van Damme, M., Whitburn, S., Clarisse, L., Clerbaux, C., Hurtmans, D., and Coheur, P. F.: Version 2 of the IASI NH_3 neural network retrieval algorithm: near-real-time and reanalysed datasets, Atmos Meas Tech, 10, 4905-4914, 10.5194/amt-10-4905-2017, 2017.

Van Damme, M., Clarisse, L., Whitburn, S., Hadji-Lazaro, J., Hurtmans, D., Clerbaux, C., and Coheur, P. F.: Industrial and agricultural ammonia point sources exposed, Nature, 564, 99-+, 10.1038/s41586-018-0747-1, 2018.

Warner, J. X., Wei, Z. G., Strow, L. L., Dickerson, R. R., and Nowak, J. B.: The global tropospheric ammonia distribution as seen in the 13-year AIRS measurement record, Atmos. Chem. Phys., 16, 5467-5479, 10.5194/acp-16-5467-2016, 2016.

Warner, J. X., Dickerson, R. R., Wei, Z., Strow, L. L., Wang, Y., and Liang, Q.: Increased atmospheric ammonia over the world's major agricultural areas detected from space, Geophys. Res. Lett., 44, 2875-2884, 10.1002/2016gl072305, 2017.

Yu, F. Q., Nair, A. A., and Luo, G.: Long-Term Trend of Gaseous Ammonia Over the United States: Modeling and Comparison With Observations, J. Geophys. Res. Atmos., 123, 8315-8325, 10.1029/2018jd028412, 2018.

https://doi.org/10.5194/acp-2019-1026
Preprint. Discussion started: 20 December 2019

Table 1. Regional Mean NH_3 Total Columns and Emissions Fluxes of NH_3, SO_2, and NO_x of the IGP and the NCP in Summer 2010.

	NH_3 total columns[a] (molecules cm^{-2})	Emissions fluxes[b] (t km^{-2} month^{-1})		
		NH_3	SO_2	NO_x
IGP	7.6×10^{16}	0.4	0.3	0.3
NCP	4.1×10^{16}	0.7	1.1	1.3

325 [a] NH_3 total columns were derived from IASI measurements

[b] Emissions fluxes were estimated using the MIX database

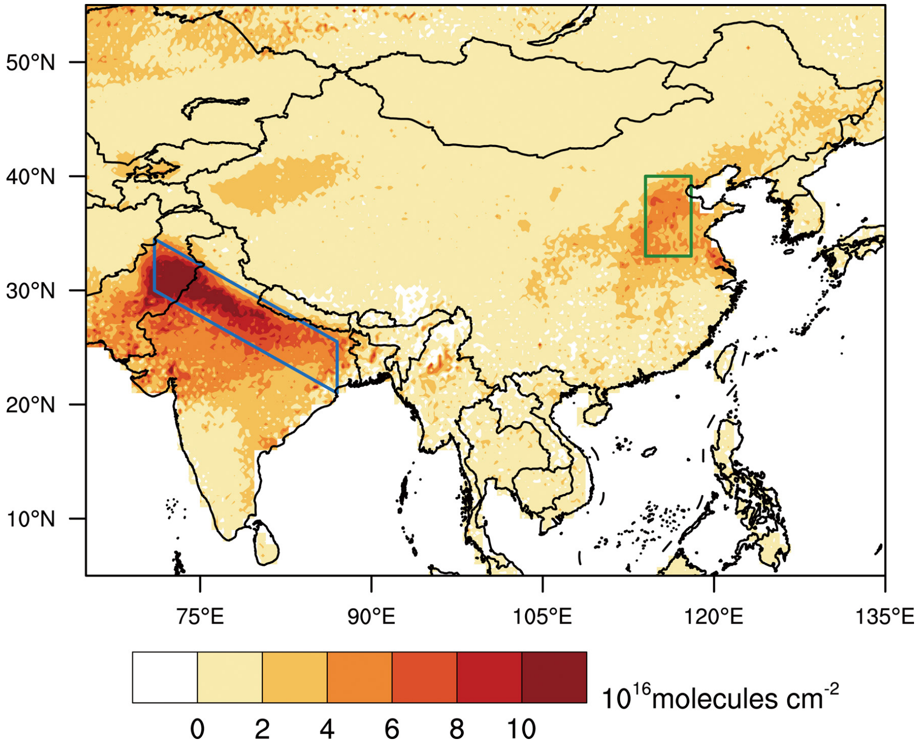

Figure 1. The spatial distribution of NH_3 total columns over East Asia in summer 2010 retrieved from 330 IASI measurements. The blue quadrangle represents the Indo-Gangetic Plain (IGP), and the green quadrangle represents the Northern China Plain (NCP).

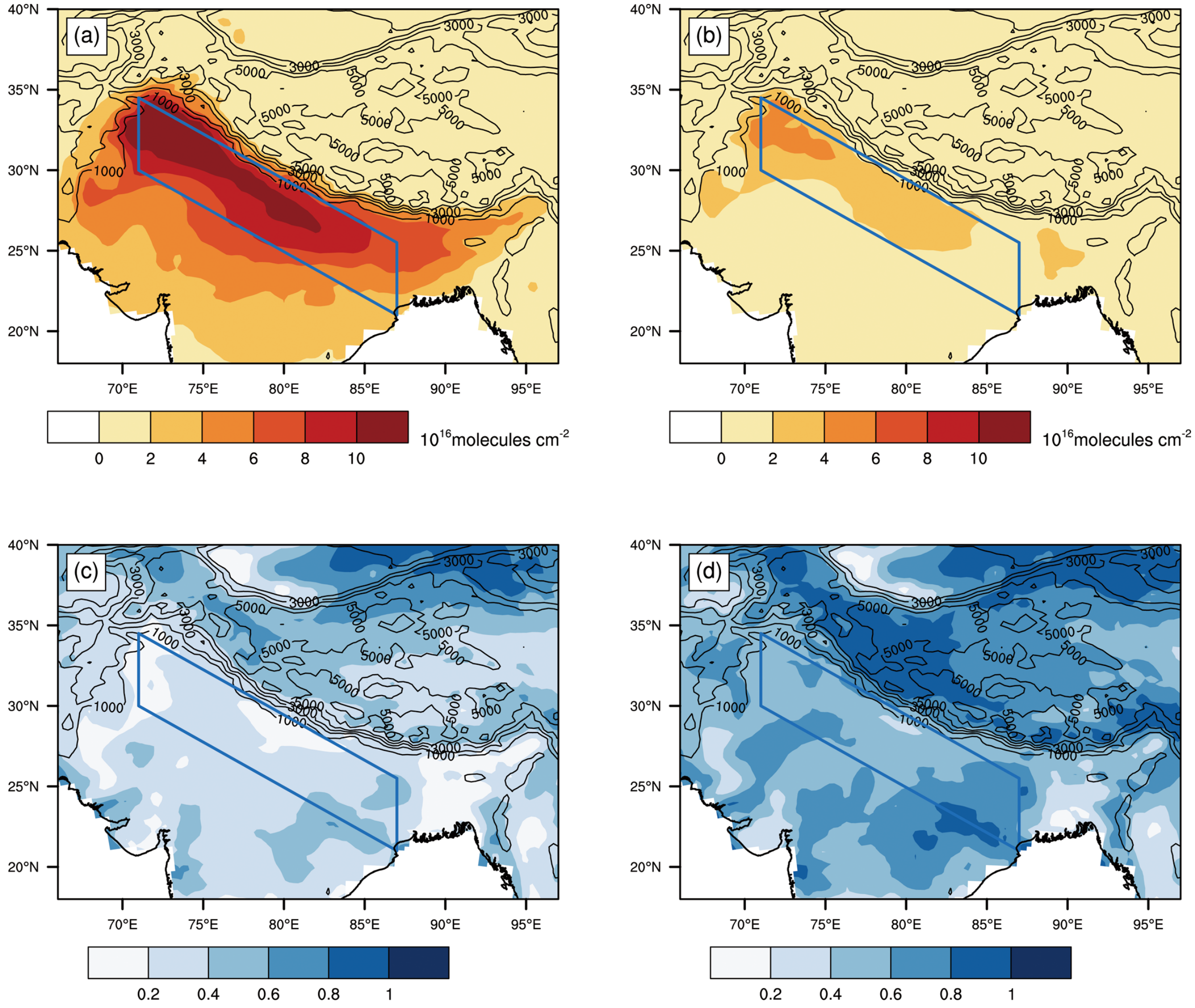

Figure 2. Spatial distributions of WRF-Chem predicted total columns of NH_3 and surface $\varepsilon(NH_4^+)$ in summer 2010. (a) and (b) are total columns of NH_3 in the base case and the increased SO_2/NO_x emissions case, respectively. (c) and (d) are surface $\varepsilon(NH_4^+)$ in the base case and the increased SO_2/NO_x emissions case, respectively.

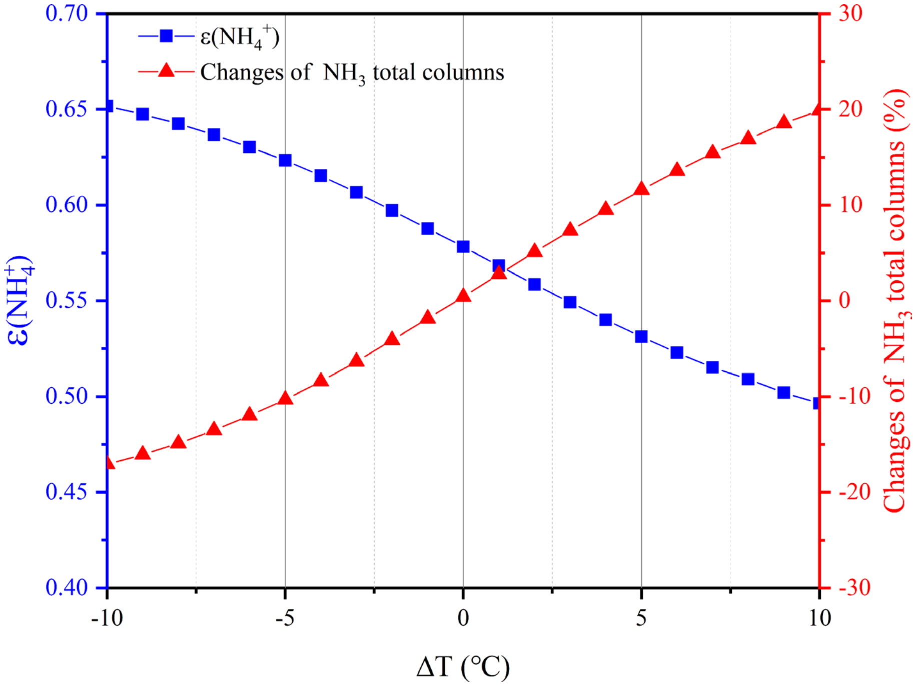

340 **Figure 3.** Columnar $\varepsilon(NH_4^+)$ and changes of NH_3 total columns with the changes of temperatures predicted by ISORROPIA-II.

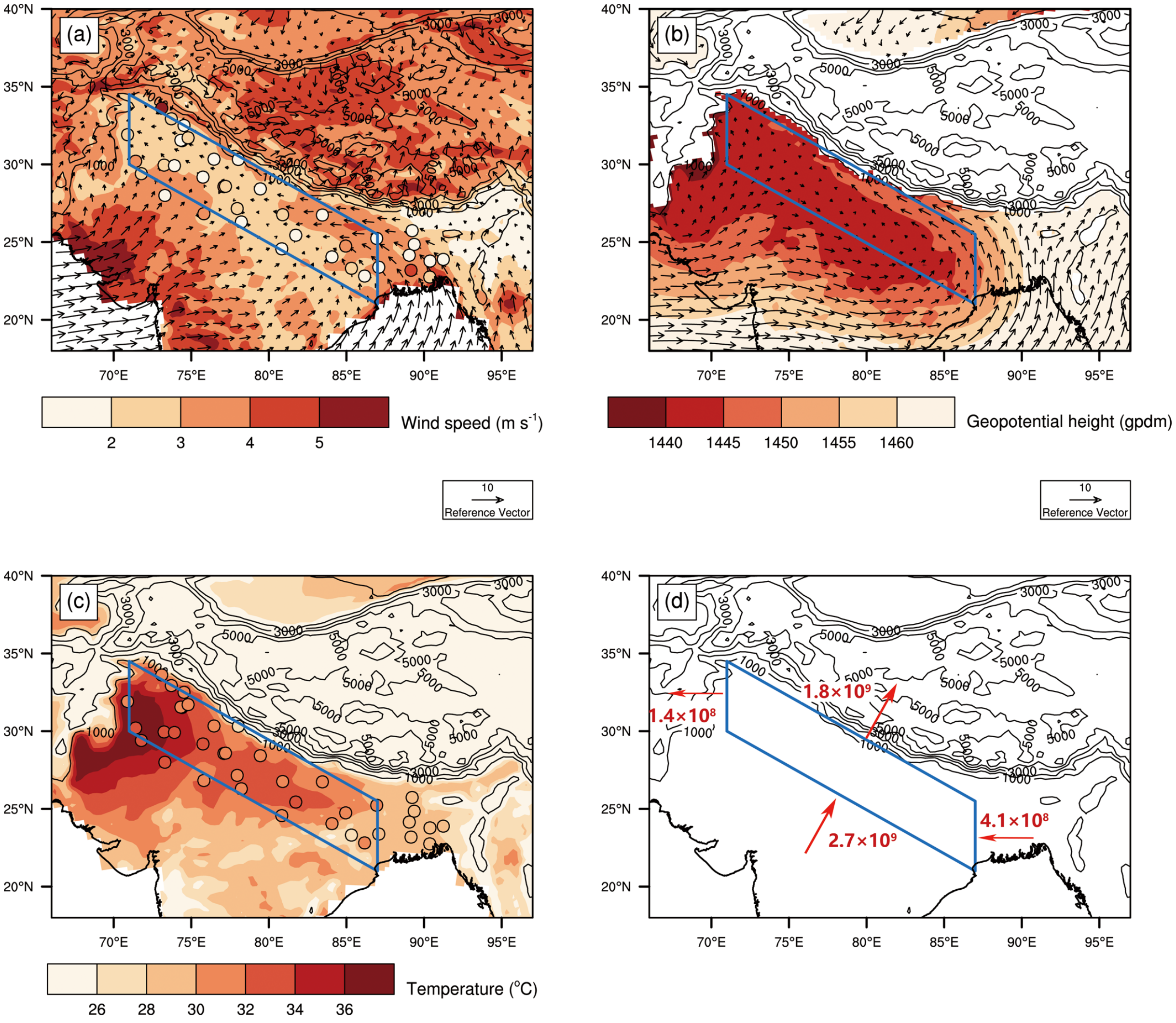

Figure 4. Spatial distributions of WRF-Chem predicted meteorological variables in summer 2010. (a) Wind flow and wind speed at 10 m. (b) Wind flow and geopotential height at 850 hPa. (c) Air temperature at 2 m. (d) Ventilation rate (m^3 s^{-1}) of the four edges of the IGP. Circles in (a) and (c) show the observed wind speed at 10 m and air temperature at 2 m, respectively.

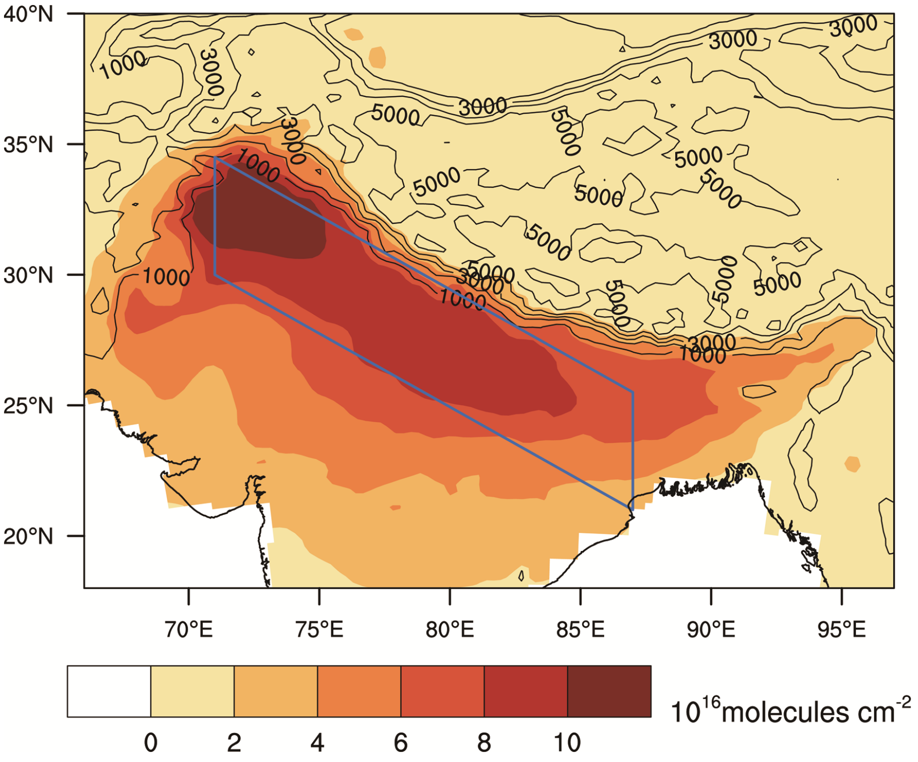

Figure 5. Spatial distributions of WRF-Chem predicted total columns of NH_3 in summer 2010 in the homogeneous emissions case.